Available online at www.sciencedirect.com
ScienceDirect
Earth and Planetary Science Letters 256 (2007) 264–277
EPSL
www.elsevier.com/locate/epsl

Evidence for recurrent Early Triassic massive volcanism from quantitative interpretation of carbon isotope fluctuations

Jonathan L. Payne [a,*], Lee R. Kump [b]

[a] Department of Geological and Environmental Sciences, Stanford University, Stanford, CA 94305, United States
[b] Department of Geosciences, The Pennsylvania State University, University Park, PA 16802, United States

Received 7 September 2006; received in revised form 26 January 2007; accepted 27 January 2007
Available online 3 February 2007
Editor: M.L. Delaney

Abstract

Carbon cycle disturbance associated with mass extinction at the end of the Permian Period continued through the Early Triassic, an interval of approximately 5 million years. Coincidence of carbon cycle stabilization with accelerated Middle Triassic biotic recovery suggests a link between carbon cycling and biodiversity, but the cause of Early Triassic carbon isotope excursions remains poorly understood. Previous modeling studies have focused exclusively on the initial negative excursion in $\delta^{13}C$ across the Permian–Triassic boundary and have not addressed the cycles of positive and negative excursions observed through the Early Triassic. This study uses a simple carbon cycle box model to investigate potential causes underlying the series of Early Triassic carbon isotope excursions and to assess possible relationships between isotope excursions and coeval patterns of carbonate deposition. According to the model, introduction of carbon with the isotope composition of volcanic CO_2 produces small negative carbon isotope excursions followed by larger and more protracted positive excursions. Positive excursions result because increased pCO_2 causes warming, enhancing marine anoxia and associated regeneration of phosphate and thus allowing greater productivity. In addition, carbonate weathering is more sensitive than organic carbon weathering to changes in atmospheric pCO_2 and climate, causing an increase in the overall $\delta^{13}C$ composition of weathered carbon. Therefore, the full Early Triassic record of negative and positive carbon isotope excursions can only be accounted for within the model by several pulses of carbon release characterized by varying mixtures of organic and mantle isotope compositions. Thermal metamorphism of coal and carbonate rocks in the crust of the Siberian craton during eruption of the Siberian Traps flood basalts provides the most plausible mechanism for such a carbon release scenario. If multiple episodes of CO_2 release account for Early Triassic carbon cycle instability (regardless of their precise trigger), then cessation of CO_2 release is likely to explain acceleration of biotic recovery early in the Middle Triassic.

Keywords: mass extinction; carbon cycle; Permian; Siberian Traps; flood basalt

1. Introduction

Multiple observations reflect disturbance of the global carbon cycle coincident with end-Permian mass extinction. Primary evidence for carbon cycle perturbation comes from the large negative excursion in $\delta^{13}C$ of carbonates and organic matter beginning near the extinction horizon [1–4]. Substantial changes in the style of shallow marine carbonate deposition also occurred globally across the Permian–Triassic boundary (PTB) [5]. In particular, widespread oolites [6] and

* Corresponding author. Tel.: +1 650 725 1602; fax: +1 650 725 0979.
E-mail address: jlpayne@stanford.edu (J.L. Payne).

0012-821X/$ - see front matter © 2007 Elsevier B.V. All rights reserved.
doi:10.1016/j.epsl.2007.01.034

precipitated microbialites containing aragonite fans [7–10] suggest disturbance beyond mere isotope effects [5]. Facies and geochemical evidence for marine anoxia [11–13], even in shallow water settings [14,15], and substantial warming in polar regions [16] is difficult to account for in the absence of elevated atmospheric pCO_2. Finally, selective extinction of marine organisms susceptible to hypercapnia (i.e., CO_2 narcosis) [17] indicates a causal relationship between carbon cycle disturbance and biological extinction. Although anoxia [18], hypercapnia [17], and hydrogen sulfide poisoning [19] have all been proposed as proximal causes of extinction, each is likely to require increased atmospheric pCO_2 to generate the conditions required to cause widespread biological harm. Moreover, these physiological stresses can act synergistically and thus need not be thought of simply as alternative kill mechanisms [20]. In short, carbon cycle disturbance appears to have played a central role regardless of the precise end-Permian kill mechanism(s).

Subsequent to the extinction event, a series of negative and positive excursions in the $\delta^{13}C$ of carbonates occurred during the Early Triassic [1,21], an interval of approximately 5 Ma [22,23]. Positive excursions reached $\delta^{13}C$ values as high as +8‰ and negative excursions went as low as −3‰ in marine carbonates (Fig. 1) [1,21,24]. Close correspondence of records from South China [1], Turkey [25], and elsewhere across Tethys [21,26] indicates that excursions reflect global carbon cycle changes [26–28]. The first two large positive excursions reached maxima near the Dienerian–Smithian and Smithian–Spathian substage boundaries and the last major positive excursion peaked early in the Anisian stage [1,21,26]. The most pronounced intervening negative excursion occurred during the Smithian [1,21,26]. Excursions lasted, on average, approximately 500 ky, although precise time constraints on individual excursions are lacking. Fig. 1 illustrates $\delta^{13}C$ data of Payne et al. [1] from southern China because it is the most detailed Early–Middle Triassic $\delta^{13}C$ record from a single locality, but comparison to other studies indicates this record is broadly representative of global patterns [1,26,27]. Carbonate rock fabrics such as precipitated carbonate microbialites, aragonite fans, and giant ooids are widespread in the immediate aftermath of the extinction and recur within younger Lower Triassic strata [29,30]. The Early Triassic was also characterized by delayed biotic recovery [31]; shallow marine benthic communities experienced only limited increase in diversity, ecological structure, and the size of organisms [32–36]. Conditions set in place at the time of extinction appear to have persisted or recurred through the Early Triassic. Therefore, explanations for Early Triassic carbon isotope excursions may shed light not only on mechanisms underlying delayed biotic recovery but also on the cause(s) of the mass extinction.

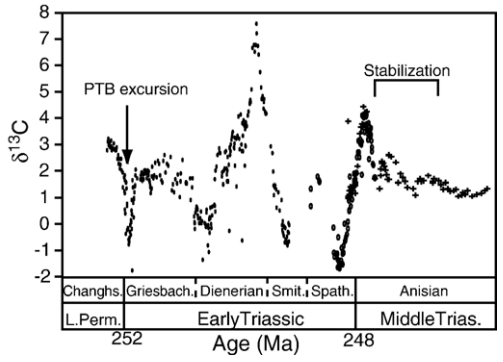

Fig. 1. Composite $\delta^{13}C$ record from the Upper Permian through Middle Triassic compiled from stratigraphic sections on the Great Bank of Guizhou, an isolated Late Permian to Middle Triassic carbonate platform in the Nanpanjiang Basin of southern China. Data are from [1]. Symbols are used to indicate data from the same stratigraphic section. Abbreviations: Changhs. — Changhsingian; Griesbach. — Griesbachian; Smit. — Smithian; Spath. — Spathian; L. Perm. — Late Permian; Trias. — Triassic.

Numerous hypotheses have been proposed to explain the boundary excursion in $\delta^{13}C$: overturn of a stratified ocean with isotopically light deep waters [17], release of isotopically light methane during destabilization of methane clathrates [37–39] or thermal metamorphism of coal measures [40,41], drastic reduction of organic carbon burial in the aftermath of extinction [42], increase in organic-carbon weathering [43], collapse of the biological pump [44], and subaerial diagenetic alteration [45] (although diagenesis was later rejected by the same author [46]). Mass balance calculations [39] and carbon cycle box models [38,42,44] generally favor the oxidation of light carbon from sedimentary reservoirs to account for the $\delta^{13}C$ excursion, although collapse of the isotope gradient within the water column can also account for this feature [44].

Early Triassic geochemical and paleontological records pose additional challenges to modeling efforts. Repeated carbon isotope perturbations through the Early Triassic are incompatible with methane release from seafloor gas hydrates because insufficient time is available between events for regenerating methane clathrates [1], although one cannot rule out the release of methane as a primary driver for any one excursion, particularly the Permian–Triassic boundary excursion [37,38]. The Early–Middle Triassic carbon isotope

record has not been the focus of any previous modeling studies. Moreover, little is known regarding the precise stratigraphic and temporal relationships among Early Triassic biological events, the occurrences of particular carbonate facies (e.g., microbialites, aragonite fans, and large ooids) and carbon isotope fluctuations. Both extinction and recovery are intimately linked with carbon cycle behavior as recorded in the geochemical and sedimentological records [1,5]. Improved understanding of these links and improved resolution of combined geochemical and paleontological records are essential to achieving satisfactory understanding of extinction and recovery processes.

In this study, building upon previous models of Berner [38] and Grard et al. [42], we investigated potential relationships between changes in carbon isotopes and carbonate sedimentology through the Early Triassic using a simple carbon cycle box model. We focused on the potential influence of carbon released from volcanism and the oxidation of organic matter and methane on the isotope composition of carbon in the oceans and on the carbonate alkalinity and carbonate saturation state of the oceans. We also compared the pattern and timing of carbon isotope change under disturbance scenarios to the pattern of change in carbonate alkalinity and carbonate saturation state – important factors in carbonate sedimentation – by tracking the carbonate alkalinity of seawater in the model. The specific goals of the study were to: (1) provide quantitative constraints on explanations for the observed Early Triassic carbon isotope record; and (2) investigate potential coupling between carbon isotope excursions and patterns of carbonate sedimentation through changes in seawater carbonate chemistry.

2. Model description

The model used in this study is a one-box ocean model describing the global organic and inorganic carbon cycles and their isotope compositions and including mass balance equations for carbonate alkalinity, phosphate, and oxygen. The model structure is illustrated schematically in Fig. 2. As a simplified model, it was intended not to explain observed data in detail but, rather, to outline the range of scenarios compatible with observations that should be targeted for more detailed future field and modeling studies. Parameterization of the model is described briefly below. A complete list of equations and parameter values used for the model is available as supplementary online material.

The model tracks organic and inorganic carbon input from weathering, CO_2 release from volcanism, and carbon release from the oxidation of reduced sedimentary carbon reservoirs such as organic matter and methane clathrates. Carbon is removed from the ocean–atmosphere system through organic and inorganic carbon burial. Carbonate alkalinity is delivered to the oceans via silicate and carbonate weathering and carbonate alkalinity is removed from the oceans via carbonate burial. Atmospheric carbon dioxide is calculated at each (1000 y) time step assuming equilibrium with the total carbon in the ocean–atmosphere system and carbonate alkalinity (see supplementary online material) [47]. In our model runs, atmospheric carbon dioxide was set to an initial equilibrium value of 1500 ppm, in accord with Berner and Kothavala's [48] estimate of atmospheric pCO_2 from GEOCARB III. The dependence of carbonate and silicate weathering fluxes

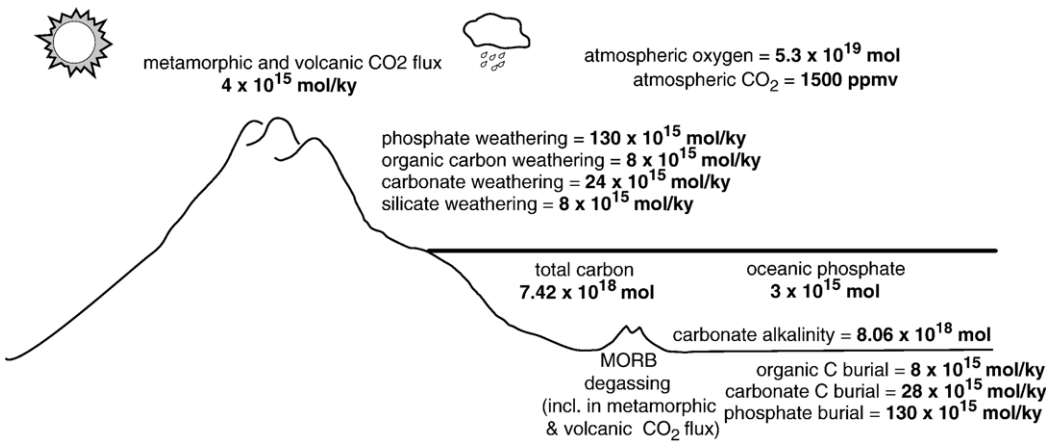

Fig. 2. Schematic illustration of the carbon cycle model used in this study. The complete set of steady state values and equations is provided in the supplementary online materials.

on temperature and runoff is parameterized following Berner's carbon cycle model [49] (see supplementary online material). Change in global average temperature is calculated as function of atmospheric pCO_2, following Walker et al. [50] (see supplementary online material). Carbonate depositional flux is parameterized as a function of the difference between carbonate alkalinity and total carbon — an approximation of the carbonate ion concentration [51].

Organic carbon burial is modeled to be proportional to phosphate availability, assuming phosphate limitation on primary productivity and organic carbon burial at the timescale of the model. Because phosphate is preferentially recycled from sediments into the water column relative to carbon under anoxic conditions [52], the burial ratio of organic carbon to phosphate is allowed to vary following a sigmoidal curve from approximately the Redfield ratio (C:P = 130) to 31 times the Redfield ratio as a function of the change in global average temperature — a crude proxy for anoxia. Higher global average temperatures tend to favor anoxia by reducing the solubility of O_2 in seawater, an effect observed in GCM simulations [e.g., [53]].

Organic carbon weathering and organic carbon burial are assumed to be the only sink and source, respectively, for oxygen. In this regard, our neglect of the sulfur cycle is an important area for future refinement. Parameterization of organic carbon burial is focused on marine processes, thus neglecting important differences between marine and terrestrial organic carbon burial. However, the absence of Early Triassic coal deposits globally suggests burial of terrestrial organic carbon was limited, with little variability [54]. The model assumes organic carbon weathering to be constant through time (aside from specified releases from sedimentary reduced carbon reservoirs) because field observations and modeling indicate quantitative oxidation of all organic carbon made available via tectonic uplift [55]. It is beyond the scope of available data to parameterize tectonic supply of sediment at the timescale of the model and therefore this factor is assumed to have been constant through the interval investigated.

3. Results

We used model experiments to investigate the behavior of the global carbon cycle in response to three separate forcings: volcanism, oxidation of organic carbon, and oxidation of biogenic methane. We then explored combined scenarios in an attempt to reproduce the observed Late Permian through Middle Triassic carbon isotope record. Within each experiment, several permutations were run to test the sensitivity of the model to disturbance parameters.

3.1. Single perturbation by volcanism

3.1.1. Scenario description

Siberian Trap volcanism is one obvious source of potential carbon cycle disturbance during the Early Triassic [41,56–59]. The original volume of erupted material is somewhat uncertain. Including the recently discovered basalts in the West Siberian Basin, it is likely to be on the order of 3×10^6 km^3 [60,61]. If the concentration of degassed CO_2 from trap eruptions was similar to values measured at the Kilauea volcano (1.5×10^{-3} mol C/cm^3 melt) [62], then 3×10^{18} mol (or approximately 30 000 Gt where 1 Gt = 10^{15} g) would reflect a reasonable estimate of CO_2 release from Siberian Trap volcanism. If thermal metamorphism and decarbonation of carbonates and organic carbon (e.g., coal seams) by mafic flows and sills enhanced volatile release [41,60], then the amount of CO_2 released may have been substantially larger [41]. To investigate the potential effects of these eruptions, we modeled the release of 3×10^{18} mol of volcanogenic CO_2 ($\delta^{13}C = -5\%$) over periods of 100, 300, and 600 ky. Eruption over 100 ky represents a reasonable lower limit on the duration of the Siberian Trap eruptions, whereas 600 ky is an intermediate value [56]. Eruption over longer timescales produce smaller excursions than that illustrated for the 600 ky scenario.

3.1.2. Model results

Fig. 3 illustrates the evolution of $\delta^{13}C$ in seawater under the 100 ky and 600 ky eruption scenarios. Results for the 300 ky scenario are intermediate and are therefore not presented. The carbon isotope response to this type of perturbation is a negative excursion followed by a positive excursion of longer duration.

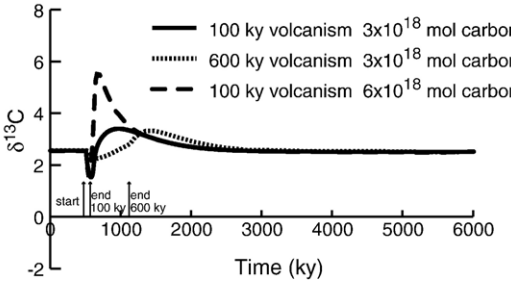

Fig. 3. Carbon isotope records from model runs involving the release of volcanogenic CO_2. Interval of carbon release indicated by a gray bar.

Because the total quantity of CO_2 release was held constant, shorter eruptive duration was associated with greater eruptive flux of CO_2, yielding a larger initial negative excursion. Rather than enhancing the negative excursion, doubling the eruptive flux reduced the duration of the negative excursion and amplified the subsequent positive carbon isotope excursion because higher atmospheric pCO_2 increased the development of anoxia and recycling of phosphate, thus enhancing organic carbon burial (Fig. 3).

Carbon isotope response is controlled by changes in both weathering and burial processes. Fig. 4 illustrates the organic and carbonate burial and weathering fluxes (Fig. 4A), the fraction of organic carbon in burial ($f_{org\ burial}$) and weathering fluxes (not including volcanogenic CO_2) ($f_{org\ weathering}$) (Fig. 4B) for the 100 ky, 3×10^{18} mol scenario. The carbonate weathering flux increased in response to increased atmospheric pCO_2 (Fig. 4A) because the carbonate weathering rate depended on runoff and temperature in the model, both functions of pCO_2. The resulting decrease in the proportional weathering of organic carbon (Fig. 4B) led

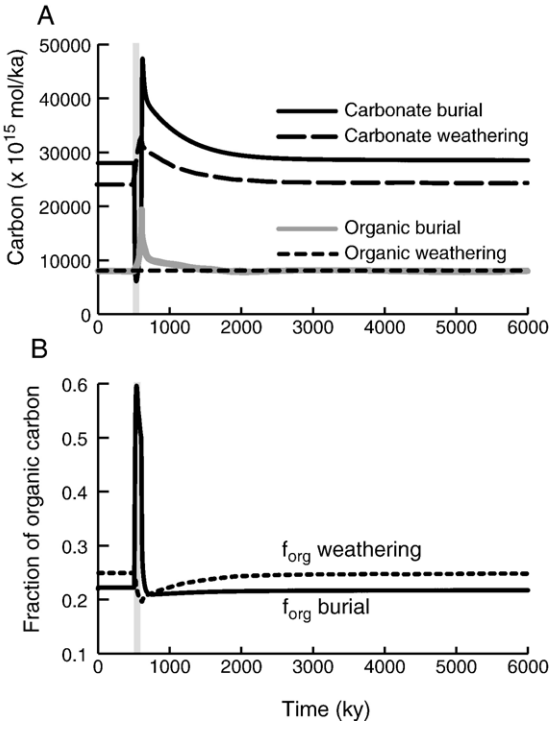

Fig. 4. Organic and inorganic carbon weathering and burial fluxes under the release of 3×10^{18} mol C over 100 ky. Interval of carbon release indicated by a gray bar. A) Organic carbon and carbonate burial and weathering fluxes. B) Fraction of carbon burial and weathering (not including volcanogenic CO_2) in the form of organic carbon.

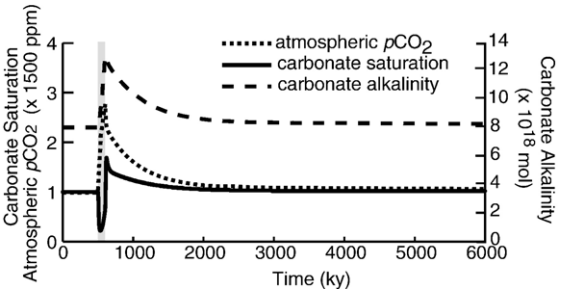

Fig. 5. Effects of volcanic release of 3×10^{18} mol C over 100 ky on marine carbonate chemistry and atmospheric pCO_2. Interval of carbon release indicated by a gray bar. Carbon isotope record for this scenario presented in Fig. 3.

to an increase in $\delta^{13}C$ of weathered carbon. The carbonate burial flux initially decreased in response to increased atmospheric pCO_2 because total carbon increased more rapidly than carbonate alkalinity, leading to decreased carbonate saturation (Fig. 5), despite an immediate increase in carbonate alkalinity (Fig. 5). Organic carbon burial increased (Fig. 4A) due to buildup of oceanic phosphate concentrations. Increased weathering, driven by increased atmospheric pCO_2, led to an increase in phosphate delivery to the oceans, increasing organic carbon burial. Further increase in organic carbon burial was permitted by the preferential recycling of phosphate under anoxic conditions. For a given total release of CO_2, more rapid release resulted in higher maximum atmospheric pCO_2 and, thus, enhanced anoxia, greater phosphate recycling, and higher rates of organic carbon burial. In short, the initial response of burial processes was toward a greater proportion of organic carbon burial and heavier values of $\delta^{13}C$ (Fig. 4A). As carbonate alkalinity built up, the rate of $CaCO_3$ burial eventually increased above the steady state value, thus driving $\delta^{13}C$ in the oceans to lighter values and providing a negative feedback to return the system to steady state. Accounting for weathering and burial of inorganic and organic carbon separately suggests that the overall response to a large and rapid input of CO_2 with a mantle isotope composition ($\delta^{13}C$ near −5‰) is likely to be a short-lived negative excursion of 1‰ or less followed by a more pronounced positive excursion of potentially a few permil [63]. The reaction of the carbon cycle to a rapid addition of CO_2 initially pushed the ocean toward a heavier carbon isotope composition – opposing the influence of the addition of light carbon. Enhanced silicate weathering and resulting increase in the $CaCO_3$ burial flux eventually returned the system to steady state by sequestering the added carbon.

In the 100 ky (3×10^{18} mol C) scenario, carbonate alkalinity of seawater and carbonate saturation state exhibited significant change in response to the volcanic CO_2 flux (Fig. 5). Following within 100–200 ky of the initial depression in carbonate saturation, sufficient added carbon had been converted to carbonate alkalinity via silicate weathering to increase the carbonate saturation state to nearly twice its steady-state value (Fig. 5). The increase and maximum in carbonate weathering preceded the increase and maximum in carbonate burial (Fig. 4), enhancing the magnitude of the positive excursion (driven primarily by elevated organic carbon burial) (Figs. 3, 5). Atmospheric pCO_2 reached 4000 ppm, then decayed toward steady state after the additional volcanic carbon flux ended (Fig. 5). Although the carbon cycle model is greatly simplified, it suggests that patterns of carbonate deposition which respond to global changes in carbonate alkalinity and saturation state may leave a characteristic signature in its temporal relationship to the isotope excursion, with the maximum rate of carbonate deposition occurring prior to the peak in $\delta^{13}C$, at least under the parameterization considered in this example. The temporal offset may be large enough to be detected if it affects patterns of carbonate deposition in globally identifiable ways (see Section 4. Discussion).

3.1.3. Sensitivity to anoxia

Atmospheric oxygen concentration, productivity, and circulation affect oceanic oxygen content [64] through effects on oxygen solubility, oxygen consumption, and oxygen supply, respectively. Oxygen solubility is a function of temperature and, therefore, increased global temperature at sites of deep water formation can cause decreased oxygen content of seawater. The preferential recycling of phosphate into the water column during organic burial under anoxic conditions provides a potential positive feedback on organic carbon burial [52]; it allows marine productivity to continue unabated even at high rates of organic carbon burial. Enhanced organic carbon burial resulting from phosphate recycling could then exaggerate positive excursions in $\delta^{13}C$. Fig. 6 illustrates the $\delta^{13}C$ evolution of seawater under two parameterizations of the C:P burial ratio (Fig. 6) for the 100 ky, 3×10^{18} mol eruption scenario. Differences in parameterization account for uncertainty in the magnitude of the interaction between increased temperature, oxygen solubility, productivity, and the mixing rate of the oceans. Under the more sensitive parameterization (lower threshold for anoxia and increased C:P), the positive excursion in $\delta^{13}C$ is both more rapid and of greater amplitude (Fig. 6) due to the increased role of

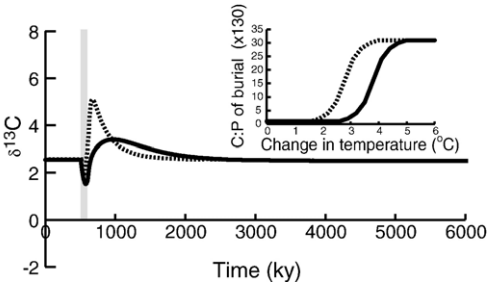

Fig. 6. Carbon isotope composition of buried carbonates and its relationship to the C:P burial ratio under two different parameterizations of C:P burial rations as a function of change in temperature. Change in temperature is a function of the change in atmospheric pCO_2 (see supplementary online materials). Scenario considered is the release of 3×10^{18} mol C over 100 ky.

phosphate recycling in enhancing organic carbon burial. Because organic carbon burial provides a negative feedback on atmospheric pCO_2, the positive excursion also ends more rapidly under the high sensitivity scenario. As this example illustrates, the sensitivity of C:P burial ratios to environmental changes (atmospheric pCO_2, temperature, etc.) helps to control the isotope response to disturbance of a given magnitude. The large difference in model results between the two parameterizations suggests that the model, and perhaps the carbon cycle itself, are contingent upon the sensitivity of marine anoxia to boundary conditions of climate and continental configuration. The sensitivity of the system need not remain constant through time, and so there is unlikely to be a single parameterization that accurately captures the behavior of the system over any extended interval of geological time.

3.2. Single perturbation by oxidized organic matter

3.2.1. Scenario description

After starting the model at steady state, we perturbed it by adding 2×10^{18} mol (approximately 20 000 GT) of oxidized organic carbon ($\delta^{13}C=-25‰$) over 100 ky and 10^{18} mol over 20 ky. On the order of 1000 km^3 of sedimentary organic carbon are required to release 10^{18} mol C (or 10 000 km^3 of coal to produce an equivalent quantity of thermogenic methane, assuming 10% efficiency of carbon release). Economic coal seams alone represent on the order of 1000 km^3 in the upper Paleozoic Tungusskaya series, and preserved carbonate-rich upper Paleozoic sediments of the Tungusskaya series represent approximately 300 000 km^3 [65]. It appears likely that hundreds or, perhaps, even thousands of Siberian Traps flows and sills approach the total volume of coal required to release 2×10^{18} mol C [41],

indicating that thermal metamorphism during intrusion and eruption could account for significant carbon release in the Early Triassic.

3.2.2. Model results

The release of organic matter caused a negative excursion in $\delta^{13}C$ of approximately 4‰ in the 100 ky scenario and 3‰ in the 20 ky scenario (Fig. 7A, B). The lighter isotopic composition of organic carbon and smaller quantity of carbon released in comparison to the volcanism scenarios damped the magnitude of the positive excursion that followed the initial negative excursion in the volcanism scenarios to less than 1‰. The positive excursion was damped due to more limited development of anoxia and more limited effects on carbonate weathering. The more rapid release of carbon in the 20 ky scenario caused a more severe decrease in saturation state than the 100 ky scenario due to the higher flux of carbon release, but caused a smaller subsequent increase in saturation state due to the smaller total quantity released and smaller effect on carbonate and silicate weathering (Fig. 7C, D). Changes in carbonate alkalinity were smaller in the 20 ky scenario due to the smaller quantity of carbon released and the consequently smaller weathering pulse that followed (Fig. 7C, D). Maximum atmospheric pCO_2 was approximately equal for the two scenarios, but elevated pCO_2 persisted substantially longer in the 100 ky scenario due to the greater quantity of carbon released and longer timescale of release (Fig. 7C, D).

3.3. Single perturbation by methane

3.3.1. Scenario description

After starting the model at steady state, we perturbed it with the addition of 5×10^{17} mol carbon (approximately 5000 GT) over 20 ky using the isotope composition of biogenic methane from seafloor clathrates ($\delta^{13}C=-60$‰). The precise amount of methane stored in seafloor clathrates is poorly constrained, but this amount is likely within a factor of two of the total quantity of seafloor clathrates that currently exist [66]. Due to isotope constraints, the quantity of methane introduced is necessarily smaller than the modeled release of organic carbon and much smaller than the modeled release of volcanogenic CO_2. The methane release scenario has previously been chosen as a preferred explanation for the PTB negative carbon isotope excursion based on field observations [37,67] and mass balance calculations [38,39].

3.3.2. Model results

The addition of methane caused a rapid negative excursion in $\delta^{13}C$ of approximately 3‰ (Fig. 8A). The isotope perturbation decayed away over the course of approximately 300 ky (Fig. 8A). Carbonate saturation

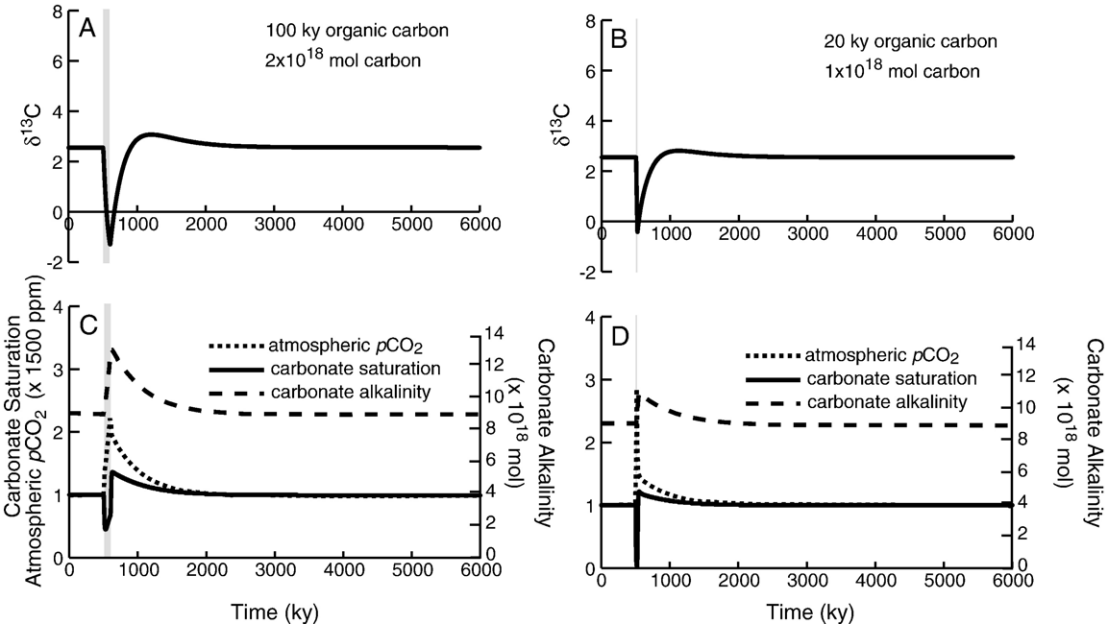

Fig. 7. Effects of the release organic carbon. Interval of carbon release is marked with a gray bar. A, C) Release of 2×10^{18} mol C over 100 ky. B, D) Release of 10^{18} mol C over 20 ky. A, B) Carbon isotope composition of buried carbonates. C, D) Records of carbonate saturation, carbonate alkalinity, and atmospheric pCO_2.

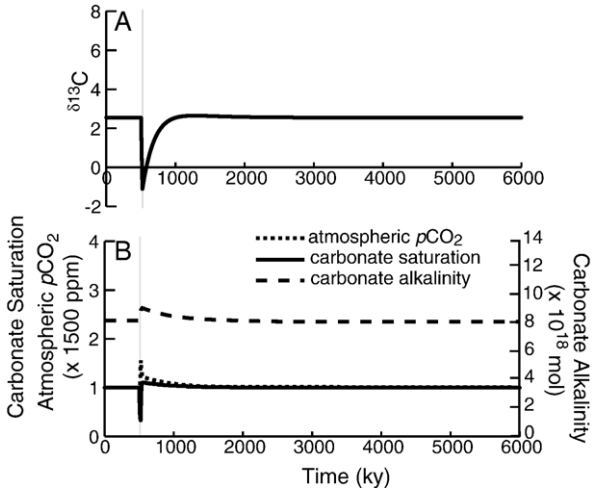

Fig. 8. Effects of the release of 5×10^{17} mol C from methane clathrates over 20 ky. Interval of carbon release is marked with a gray bar. A) Carbon isotope composition of buried carbonates. B) Records of carbonate saturation and carbonate alkalinity of the oceans, and atmospheric pCO_2.

decreased severely as a result of the carbon release (Fig. 8B), but the subsequent weathering pulse and increase in organic carbon burial were too small to cause more than a minor subsequent increase in saturation state or carbonate alkalinity (Fig. 8B). Likewise, atmospheric pCO_2 increased only to approximately 2500 ppm, about half the increase observed in the 20 ky scenario for organic carbon release. The smaller effects on carbonate saturation, alkalinity, and atmospheric pCO_2 all reflect the smaller quantity of carbon required to produce the observed carbon isotope excursion under the methane scenario.

3.4. Fitting the Early Triassic carbon isotope record

3.4.1. Model results

None of the models experiments produced multiple excursions in $\delta^{13}C$ beyond a single negative-to-positive couplet. Only the volcanism scenarios produced positive excursions in $\delta^{13}C$ of the magnitude observed in the Early Triassic record. For the model to account for the Early Triassic $\delta^{13}C$ record, several pulses of volcanic CO_2 release are required. Fig. 9A illustrates the $\delta^{13}C$ record produced by modeled episodes of organic carbon release, with an average $\delta^{13}C$ composition of −25‰, chosen to fit the timing and approximate magnitudes of the negative excursions in $\delta^{13}C$ from the Early Triassic record. We then added episodes of volcanogenic carbon release with an average $\delta^{13}C$ composition of −5‰ (Fig. 9A) to fit the observed carbon isotope record to the best degree possible. The intent of this exercise was not to identify a unique scenario to account for the full Early Triassic record; rather, it was to identify at least one scenario that is broadly consistent with the observed isotope record and available geological evidence. Moreover, $\delta^{13}C$ of −25‰ need not reflect oxidation only of organic matter but, rather, could reflect the average isotope composition of a mixture of isotopically lighter (e.g., biogenic or thermogenic methane) and heavier (e.g., volcanogenic CO_2 or carbonate rocks) sources of carbon. Fig. 9B illustrates the volcanic (−5‰) and organic carbon (−25‰) fluxes, respectively, added to the steady state model to approximate the Early Triassic record. Fig. 9C illustrates the evolution of atmospheric pCO_2 and carbonate saturation under the preferred scenario. We have presented results without methane due to concerns that the timescale for methane clathrate regeneration is too long to accommodate multiple, large releases during the Early Triassic [1]. Although the timing and magnitude of the preferred combined model run do not perfectly match the observed data, we consider the fit adequate given

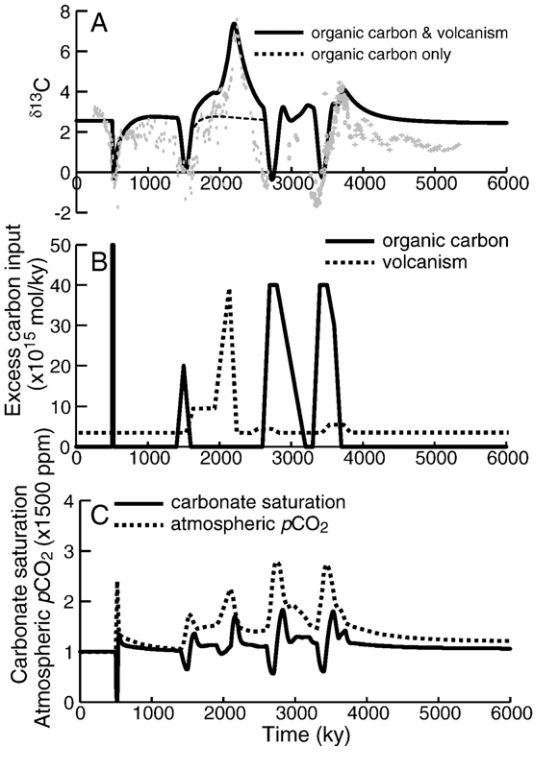

Fig. 9. A hypothetical scenario of multiple disturbances during the Early Triassic. A) Carbon isotope composition of carbonate sediments. B) Modeled volcanogenic carbon and organic carbon release fluxes. C) Records of carbonate saturation and atmospheric pCO_2 for the emission of volcanogenic and organic carbon.

uncertainties with respect to the Early Triassic timescale and magnitude of carbon isotope excursions. Substantial further improvements require refinement of the model (e.g., through parameterization of the sulfur cycle, terrestrial organic carbon burial, or sea level) or improved resolution of the Early Triassic timescale, rather than through adjustments to the proposed scenario.

3.4.2. Sensitivity to model parameterization

The model is relatively insensitive to the precise parameterization of silicate and carbonate weathering feedbacks. Adjustment of weathering sensitivity within the range of values advocated by Berner [49] does not qualitatively alter the results. Substitution of simpler weathering feedbacks employed in earlier models [e.g., [50]] also yields similar results.

Long-term modeling from isotope records suggests an approximate 50% decline in atmospheric pO_2 from the Permian to the Middle Triassic, including a 25% decline from the latest Permian through the end of the Early Triassic [68]. Such a drastic drop is not produced in the model presented above due to differences in model assumptions. It is possible to impose this decline in atmospheric oxygen on the model by decoupling atmospheric oxygen content from organic carbon burial and weathering controls assumed in the model. Such decoupling enhances organic carbon burial, particularly late in the Early Triassic as oxygen concentrations reach low values. As a result, it returns values of $\delta^{13}C$ approximately 1‰ heavier near the end of the model run, but otherwise deviations from the results present in Fig. 9 are less than 0.5‰. As indicated by Figs. 3 and 6, carbon isotope records produced by our model are most sensitive to the parameterization of the anoxia feedback.

4. Discussion

There are two classes of explanation for continued Early Triassic carbon cycle instability: continuing environmental disturbances or lingering effects from a single disturbance. Within the model considered above, we were unable to generate continuing carbon isotope excursions over the required timescale from a single disturbance. We were able to produce a record quantitatively similar to the Early–Middle Triassic carbon isotope record through multiple injections of carbon with volcanogenic ($\delta^{13}C=-5‰$) and organic ($\delta^{13}C=-25‰$) isotope signatures.

The failure of the model to produce multiple excursions in response to a single injection of carbon suggests that multiple Early Triassic events are required to explain the observed carbon isotope record. However, multiple excursions are not impossible to generate in principle. For example, Zachos and Kump [69] modeled an example of damped oscillatory behavior in the carbon cycle when interplay between silicate weathering, climate, and ice-sheet size is considered. A decrease in atmospheric pCO_2 causes a cooling that allows ice sheets to expand. As they do, silicate weathering terrains are covered, which reduces weathering and allows pCO_2 to increase. The ice sheets growth rate responds to atmospheric pCO_2 (climate) and the rate of atmospheric pCO_2 rise (buffered by the larger ocean reservoir) responds to ice sheet size. That is, each component responds to the first derivative of the other, and their time constants are similar and, thus, the system is a damped oscillator. Although more complex and realistic models may contain appropriate feedbacks to generate oscillatory behavior of the required magnitude in the Early Triassic carbon cycle, we are unaware of any existing models that do generate oscillations of the observed magnitude.

Unlike negative $\delta^{13}C$ excursions, which can be explained in multiple ways depending on magnitude and timescale [e.g., [38]], positive excursions are more difficult to account for because there are no known sources for the simple release of large quantities of ^{13}C-rich carbon. Increased carbonate weathering and organic carbon burial in response to elevated atmospheric pCO_2 and anoxia-phosphate feedbacks were the primary drivers of positive carbon isotope excursions in the model runs, but they are not the only potential mechanisms for generating positive shifts in $\delta^{13}C$ of several permil. Rapid exposure of a large area of carbonate rock, for example, could also influence the isotope composition of weathered carbon by increasing the proportional contribution of inorganic carbon to the weathering flux, as has been suggested in association with the Ashgill (Late Ordovician) glaciation [70]. In the case of the Early Triassic, however, there is no evidence for significant glaciation. Permo-Carboniferous glaciation ended within the Permian and, if anything, the Lower Triassic was warmer than the Late Permian [e.g., [16]]. Moreover, sea level was rising across the Permian–Triassic boundary and into the Early Triassic [71].

Grard et al. [42] produced a 5‰ positive excursion in their model (illustrated in their Fig. 7) as a byproduct of phosphate buildup from an 80% reduction in organic carbon burial specified for the prior 700 ky to account for the PTB negative excursion. The absence of any observed positive excursion immediately following the PTB negative excursion (Fig. 1) renders such a scenario

doubtful as the cause of the PTB negative excursion. We also view maintaining extremely low organic carbon burial for a protracted period as an unrealistic explanation for subsequent positive carbon isotope excursions because productivity should increase as phosphate builds up (unless other factors in the post-extinction ocean prevented it). In the face of increased productivity, maintaining low organic carbon burial would require decreasing burial efficiency through time — a scenario that is especially unlikely during intervals of widespread anoxia and reduced bioturbation [35,72] such as the earliest Triassic [14,15]. It does appear that terrestrial organic carbon burial decreased drastically across the Permian–Triassic boundary, but it also appears to have remained low throughout the Early Triassic [54]. Therefore, we view changes in terrestrial organic carbon burial as unlikely to account for Early Triassic carbon isotope fluctuations. The model presented in this study does not require an arbitrary imposition of temporarily reduced organic carbon burial to produce subsequent positive excursions in $\delta^{13}C$, suggesting that it may come closer to reflecting underlying carbon cycle processes. Although the effects of elevated atmospheric pCO_2 on the weathering and burial of carbon are not the only scenarios that can account for the Lower Triassic $\delta^{13}C$ record, they provide a relatively simple explanation for available data.

The models in this study and in previous studies [38,42,44] have not addressed the potential role of sea level in controlling the proportion of organic carbon in burial and weathering fluxes. Sea level is a potentially important control on both the weathering and burial of carbon – particularly to the degree that sea-level change is linked to preferential weathering of carbonates or burial of organic carbon. For example, sea level rise could flood tropical river deltas – major sites of organic carbon burial – with deep waters within the oxygen minimum zone, linking organic carbon burial to sea level [sensu [73]].

The effects on patterns of carbonate deposition predicted by changes in carbonate saturation provide a test against the geological record independent of the $\delta^{13}C$ record. The Great Bank of Guizhou in Guizhou Province, China, is a locality where sufficient data exist to test the relationship between the carbon isotope record and the occurrence of precipitated carbonate fabrics. The 20 ky release scenario preferred to explain the PTB negative excursion implies rapid reduction in carbonate saturation followed by an excursions to maximum carbonate saturation, all during the negative carbon isotope excursion, consistent with the occurrence of microbialites within the negative excursion (Fig. 10)

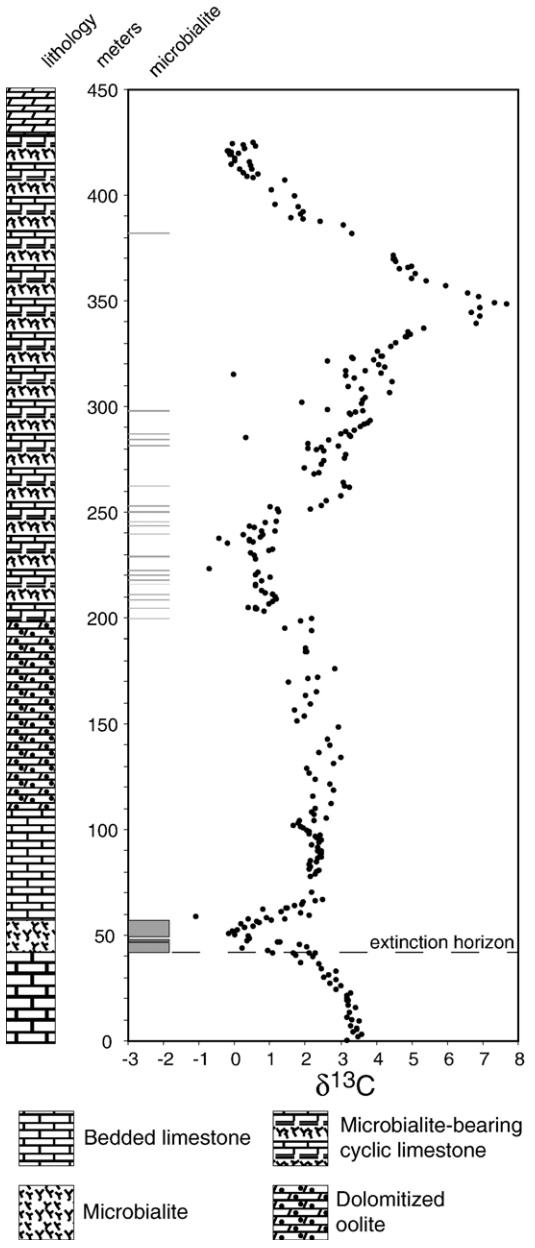

Fig. 10. Carbon isotope record from the Dajiang section in the interior of the Great Bank of Guizhou (data from [1]), an isolated Late Permian through Middle Triassic carbonate platform in South China [80]. Microbialite horizons are indicated by gray bars. Microbialites occur primarily during negative carbon isotope excursions and during increases in $\delta^{13}C$ at this site, generally consistent with predictions of high carbonate saturation at these times in modeled scenarios of carbon release.

and possible carbonate dissolution at the base of the microbialites [46]. Moreover, the coincidence of mass extinction with an abrupt negative excursion in $\delta^{13}C$ is best explained by a rapid event or series of events. Later

Early Triassic positive and negative excursions require larger, but more protracted, release of volcanogenic and organic carbon. Under these more gradual release scenarios, maxima in carbonate saturation and carbonate alkalinity occur between the initial negative excursion and the maximum of the subsequent positive excursion. Microbialites in the interior of the GBG occur primarily during the negative excursion, becoming absent before the peak of a large positive excursion in $\delta^{13}C$ (Fig. 10). If associations between carbon isotope excursions and the prevalence of certain carbonate facies are produced by events hypothesized above, then future studies should identify the same associations at widely separated localities unlikely to reflect the same local depositional controls.

As has been recognized previously [37–39], the boundary excursion in $\delta^{13}C$, taken alone, is most easily accounted for by the introduction of light carbon from organic matter or methane, given the lack of observational constraints on isotope gradients within the water column. Collapse of the biological pump, and the associated $\delta^{13}C$ gradient between shallow and deep water, can also cause a transient excursion in surface water $\delta^{13}C$ [44,74,75] without requiring cessation of organic carbon burial [74]. Scenarios involving larger and, in particular, more rapid releases of carbon are better able to account for associated extinction and the deposition of precipitated carbonate fabrics across the tropics in the immediate aftermath of the event.

The magnitude of the isotopic excursions in surface waters may have been enhanced by temporary collapse of the biological pump, but extremely low rates of marine organic carbon burial appear unlikely to explain the excursion because of the associated problem of phosphate buildup that should cause a subsequent positive carbon isotope excursion. Moreover, a low organic burial scenario does not provide any explanation for extinction or associated carbonate depositional phenomena. We currently favor a scenario of rapid release of organic carbon and volcanogenic CO_2 during Siberian Traps eruptions [sensu [40,41]] because it can account for the timing and rapidity of extinction as well as subsequent widespread deposition of oolites and precipitated carbonate microbialites. The Siberian Traps are unusual among flood basalt provinces because they were erupted through continental strata rich in coal and carbonate rocks [41]. The volume and high temperature of Siberian Traps magmas open the possibility of extensive thermal metamorphism and associated decarbonation of coal and carbonate strata in the crust [41]. Borehole observations of sedimentary strata on the Siberian Platform support the hypothesis of extensive contact metamorphism associated with igneous intrusives [76], and coal seams can be observed in outcrop to be intruded above and below by Traps-related sills (L. Elkins-Tanton, pers. comm., 2006). However, the extent and magnitude of thermal metamorphism and associated degassing of CO_2 are poorly constrained at present.

Although Siberian Traps eruptions almost certainly were occurring at the time of mass extinction [56], the extent to which eruptions continued during the Early Triassic is poorly constrained. Most of the Siberian Traps flows near Noril'sk appear to have been erupted between 252 and 251 Ma [56], but other flows and sills may be as much as several million years younger [56,77]. Because the duration of the Early Triassic is at most 5 Ma [22,23], much of the Early Triassic carbon isotope record can be accounted for even if eruptions persisted for only a few million years. Moreover, the Griesbachian to Smithian interval characterized by the largest isotope excursions may represent only the first 2 Ma or less of Early Triassic time [23]. Mundil et al. [78], using a new technique to prepare zircons that is designed to reduce the effects of lead loss, obtained a date for the Permian–Triassic extinction of 252.6 Ma, more than 1 My older than the date obtained for the extinction by Bowring et al. [79] and for the main pulse of traps eruptions by Kamo et al. [56]. Differences in sample preparation techniques between the study of Mundil et al. [78] and previous studies make it difficult to evaluate whether or not these results indicate a major pulse of traps eruptions during the Early Triassic. Some associated intrusions clearly post-date the extinction horizon [77]. However, the occurrence of sufficiently intense volcanism to drive of Early Triassic carbon isotope excursions requires additional radiometric constraints on Siberian Traps eruptions.

It is attractive to hypothesize carbon release during Siberian Traps eruptions as the primary trigger of extinction because this scenario can also account for the Early Triassic interval of carbon isotope excursions [1,21], episodic anoxia [14], and delayed biotic recovery [31] through continued carbon release. Other mechanisms proposed to account for the PTB negative $\delta^{13}C$ excursion either cannot explain all subsequent negative excursions (methane release) or leave positive excursions unaccounted for (organic carbon oxidation, methane release, collapsed biological pump). Likewise, extinction scenarios requiring a singular event (such as bolide impact) suffer from an inability to account for the series of observed carbon isotope excursions, at least until appropriate feedbacks are identified to generate multiple, large carbon isotope excursions following a single trigger.

5. Conclusions

Based upon model results, we hypothesize that the Permian–Triassic boundary excursion was produced by the introduction of approximately 10^{18} mol of carbon in less than 20 ky, most of which was derived from organic carbon within the crust rather than mantle-derived volatiles (as previously proposed by [40,41]). We hypothesize that subsequent negative and positive carbon isotope excursions resulted from larger but more protracted releases of carbon, over 100 ky or more, also associated with episodes of Siberian Traps emplacement. Variation in the proportions of carbon from coals, carbonate rocks, and Siberian Traps magmas, in addition to variations in the rate and magnitude of carbon release can account for differences in the shape and magnitude of Early Triassic carbon isotope excursions. In additional to explaining carbon isotope variations, such a scenario can account for the timing of mass extinction and the extensive deposition of Lower Triassic microbialites and carbonate precipitates, including the stratigraphic relationships between microbialites and carbon isotope excursions.

Acknowledgments

This study was funded, in part, by the NASA Astrobiology Institute (NASA cooperative agreement, grant #NNA04CC06A) and the U.S. National Science Foundation (Grant EAR-0208119) to LRK. The work was partially completed while JLP was supported on a fellowship from the Canadian Institute for Advanced Research, Earth System Evolution Program. We thank R. Berner and an anonymous reviewer for constructive comments.

Appendix A. Supplementary data

Supplementary data associated with this article can be found, in the online version, at doi:10.1016/j.epsl.2007.01.034.

References

[1] J.L. Payne, D.J. Lehrmann, J.Y. Wei, M.J. Orchard, D.P. Schrag, A.H. Knoll, Large perturbations of the carbon cycle during recovery from the end-Permian extinction, Science 305 (2004) 506–509.

[2] M. Magaritz, R. Bar, A. Baud, W.T. Holser, The carbon-isotope shift at the Permian Triassic boundary in the Southern Alps is gradual, Nature 331 (1988) 337–339.

[3] A. Baud, M. Magaritz, W.T. Holser, Permian–Triassic of the Tethys — carbon isotope studies, Geol. Rundsch. 78 (1989) 649–677.

[4] K. Wang, H.H.J. Geldsetzer, H.R. Krouse, Permian–Triassic extinction: organic $\delta^{13}C$ evidence from British-Columbia, Canada, Geology 22 (1994) 580–584.

[5] A. Baud, S. Richoz, S.B. Pruss, Lower Triassic anachronistic carbonate facies in space and time, Glob. Planet. Change 55 (2007) 81–89.

[6] J.R. Groves, M. Calner, Lower Triassic oolites in Tethys: a sedimentologic response to the end-Permian mass extinction, Geological Society of America Annual Meeting Abstracts with Program, vol. 36, 2004, p. 336.

[7] S. Kershaw, L. Guo, A. Swift, J.S. Fan, Microbialites in the Permian–Triassic boundary interval in Central China: structure, age and distribution, Facies 47 (2002) 83–89.

[8] S. Kershaw, T.S. Zhang, G.Z. Lan, A microbialite carbonate crust at the Permian–Triassic boundary in South China, and its palaeoenvironmental significance, Palaeogeogr. Palaeoclimatol. Palaeoecol. 146 (1999) 1–18.

[9] A. Baud, S. Cirilli, J. Marcoux, Biotic response to mass extinction: the lowermost Triassic microbialites, Facies 36 (1997) 238–242.

[10] E. Heydari, J. Hassanzadeh, W.J. Wade, A.M. Ghazi, Permian–Triassic boundary interval in the Abadeh section of Iran with implications for mass extinction: Part 1 — sedimentology, Palaeogeogr. Palaeoclimatol. Palaeoecol. 193 (2003) 405–423.

[11] Y. Isozaki, Timing of Permian–Triassic anoxia, Science 277 (1997) 1748–1749.

[12] P.B. Wignall, R.J. Twitchett, Permian–Triassic sedimentology of Jameson Land, East Greenland: incised submarine channels in an anoxic basin, J. Geol. Soc. 159 (2002) 691–703.

[13] Y. Kato, K. Nakao, Y. Isozaki, Geochemistry of Late Permian to Early Triassic pelagic cherts from southwest Japan: implications for an oceanic redox change, Chem. Geol. 182 (2002) 15–34.

[14] P.B. Wignall, R.J. Twitchett, Extent, duration, and nature of the Permian–Triassic superanoxic event, in: C. Koeberl, K.G. MacLeod (Eds.), Catastrophic Events and Mass Extinctions; Impacts and Beyond, Geological Society of America Special Publication, vol. 356, Geological Society of America, Boulder, Colorado, 2002, pp. 395–413.

[15] K. Grice, C.Q. Cao, G.D. Love, M.E. Bottcher, R.J. Twitchett, E. Grosjean, R.E. Summons, S.C. Turgeon, W. Dunning, Y.G. Jin, Photic zone euxinia during the Permian–Triassic superanoxic event, Science 307 (2005) 706–709.

[16] G.J. Retallack, Postapocalyptic greenhouse paleoclimate revealed by earliest Triassic paleosols in the Sydney Basin, Australia, Geol. Soc. Amer. Bull. 111 (1999) 52–70.

[17] A.H. Knoll, R.K. Bambach, D.E. Canfield, J.P. Grotzinger, Comparative Earth history and Late Permian mass extinction, Science 273 (1996) 452–457.

[18] P.B. Wignall, A. Hallam, Anoxia as a cause of the Permian Triassic mass extinction: facies evidence from northern Italy and the western United-States, Palaeogeogr. Palaeoclimatol. Palaeoecol. 93 (1992) 21–46.

[19] L.R. Kump, A. Pavlov, M.A. Arthur, Massive release of hydrogen sulfide to the surface ocean and atmosphere during intervals of oceanic anoxia, Geology 33 (2005) 397–400.

[20] H.O. Pörtner, M. Langenbuch, B. Michaelidis, Synergistic effects of temperature extremes, hypoxia, and increases in CO_2 on marine animals: from Earth history to global change, J. Geophys. Res. 110 (2005), doi:10.1029/2004JC002561.

[21] N.-V. Atudorei, Constraints on the Upper Permian to Upper Triassic marine carbon isotope curve. Case studies from the Tethys, PhD, University of Lausanne, 1999.

[22] D.J. Lehrmann, J. Ramezani, M.W. Martin, S.A. Bowring, P. Montgomery, P. Enos, J.L. Payne, M.J. Orchard, H.-M. Wang, J. Wei, Timing of biotic recovery from the end-Permian extinction: biostratigraphic and geochronologic constraints from south China, Geology 34 (2006) 1053–1056.

[23] M. Ovtcharova, H. Bucher, U. Schaltegger, T. Galfetti, A. Brayard, J. Guex, New Early to Middle Triassic U–Pb ages from South China: calibration with ammonoid biochronozones and implications for the timing of the Triassic biotic recovery, Earth Planet. Sci. Lett. 243 (2006) 463–475.

[24] A. Baud, V. Atudorei, Z. Sharp, Late Permian and early Triassic evolution of the Northern Indian margin: Carbon isotope and sequence stratigraphy, Geodin. Acta 9 (1996) 57–77.

[25] S. Richoz, Stratigraphie et variations isotopiques due carbone dans le Permien supérieur et le Trias inférieur de la Néotéthys (Turquie, Oman et Iran), Université de Lausanne, 2004.

[26] C. Korte, H.W. Kozur, J. Veizer, $\delta^{13}C$ and $\delta^{18}O$ values of Triassic brachiopods and carbonate rocks as proxies for coeval seawater and palaeotemperature, Palaeogeogr. Palaeoclimatol. Palaeoecol. 226 (2005) 287–306.

[27] H. Yin, Q. Feng, X. Lai, A. Baud, J. Tong, The protracted Permo-Triassic crisis and multi-episode extinction around the Permian–Triassic boundary, Glob. Planet. Change 55 (2007) 1–20.

[28] F.A. Corsetti, A. Baud, P.J.R. Marenco, S. Richoz, Summary of Early Triassic carbon isotope records, C. R. Palevol 4 (2005) 405–418.

[29] S.B. Pruss, D.J. Bottjer, F.A. Corsetti, A. Baud, A global marine sedimentary response to the end-Permian mass extinction: examples from southern Turkey and the western United States, Earth-Sci. Rev. 78 (2006) 193–206.

[30] S.B. Pruss, F.A. Corsetti, D.J. Bottjer, The unusual sedimentary rock record of the Early Triassic: a case study from the southwestern United States, Palaeogeogr. Palaeoclimatol. Palaeoecol. 222 (2005) 33–52.

[31] A. Hallam, Why was there a delayed radiation after the end-Paleozoic extinctions? Hist. Biol. 5 (1991) 257–262.

[32] J.L. Payne, D.J. Lehrmann, J. Wei, A.H. Knoll, The pattern and timing of biotic recovery from the end-Permian extinction on the Great Bank of Guizhou, Guizhou Province, China, Palaios 21 (2006) 63–85.

[33] M.L. Fraiser, D.J. Bottjer, The non-actualistic Early Triassic gastropod fauna: a case study of the Lower Triassic Sinbad Limestone member, Palaios 19 (2004) 259–275.

[34] J.K. Schubert, D.J. Bottjer, Aftermath of the Permian–Triassic mass extinction event — paleoecology of Lower Triassic carbonates in the western USA, Palaeogeogr. Palaeoclimatol. Palaeoecol. 116 (1995) 1–39.

[35] R.J. Twitchett, Palaeoenvironments and faunal recovery after the end-Permian mass extinction, Palaeogeogr. Palaeoclimatol. Palaeoecol. 154 (1999) 27–37.

[36] J.L. Payne, Evolutionary dynamics of gastropod size across the end-Permian extinction and through the Triassic recovery interval, Paleobiology 31 (2005) 269–290.

[37] E.S. Krull, G.J. Retallack, delta C-13 depth profiles from paleosols across the Permian–Triassic boundary: evidence for methane release, Geol. Soc. Amer. Bull. 112 (2000) 1459–1472.

[38] R.A. Berner, Examination of hypotheses for the Permo-Triassic boundary extinction by carbon cycle modeling, Proc. Natl. Acad. Sci. U. S. A. 99 (2002) 4172–4177.

[39] D.H. Erwin, The Great Paleozoic Crisis: Life and Death in the Permian, Columbia University Press, New York, 1993 327 pp.

[40] H. Svensen, S. Planke, A. Malthe-Sorenssen, B. Jamtveit, R. Myklebust, T.R. Eidem, S.S. Rey, Release of methane from a volcanic basin as a mechanism for initial Eocene global warming, Nature 429 (2004) 542–545.

[41] D.H. Erwin, Extinction: How Life on Earth Nearly Ended 250 Million Years Ago, Princeton University Press, Princeton, NJ, 2006 306 pp.

[42] A. Grard, L.M. François, C. Dessert, B. Dupré, Y. Goddéris, Basaltic volcanism and mass extinction at the Permo-Triassic boundary: environmental impact and modeling of the global carbon cycle, Earth Planet. Sci. Lett. 234 (2005) 207–221.

[43] W.T. Holser, H.P. Schonlaub, M. Attrep, K. Boeckelmann, P. Klein, M. Magaritz, C.J. Orth, A. Fenninger, C. Jenny, M. Kralik, H. Mauritsch, E. Pak, J.M. Schramm, K. Stattegger, R. Schmoller, A unique geochemical record at the Permian Triassic boundary, Nature 337 (1989) 39–44.

[44] M.R. Rampino, K. Caldeira, Major perturbation of ocean chemistry and a 'Strangelove Ocean' after the end-Permian mass extinction, Terra Nova 17 (2005) 554–559.

[45] E. Heydari, W.J. Wade, J. Hassanzadeh, Diagenetic origin of carbon and oxygen isotope compositions of Permian–Triassic boundary strata, Sediment. Geol. 143 (2001) 191–197.

[46] E. Heydari, J. Hassanzadeh, Deev Jahi Model of the Permian–Triassic boundary mass extinction: a case for gas hydrates as the main cause of biological crisis on Earth, Sediment. Geol. 163 (2003) 147–163.

[47] L.R. Kump, M. Arthur, Global chemical erosion during the Cenozoic: weatherability balances the budget, in: W. Ruddiman (Ed.), Tectonics, Uplift, and Climate Change, Plenum Press, New York, 1997, pp. 399–426.

[48] R.A. Berner, Z. Kothavala, GEOCARB III: a revised model of atmospheric CO_2 over Phanerozoic time, Am. J. Sci. 301 (2001) 182–204.

[49] R.A. Berner, The Phanerozoic Carbon Cycle: CO_2 and O_2, Oxford University Press, New York, 2004 150 pp.

[50] J.C.G. Walker, P.B. Hays, J.F. Kasting, A negative feedback mechanism for the long-term stabilization of Earth's surface-temperature, J. Geophys. Res., Oceans Atmos. 86 (1981) 9776–9782.

[51] W.S. Broecker, T.-H. Peng, Tracers in the Sea, Eldigo Press, Palisades, NY, 1982 690 pp.

[52] P. Van Cappellen, E.D. Ingall, Benthic phosphorus regeneration, net primary production, and ocean anoxia — a model of the coupled marine biogeochemical cycles of carbon and phosphorus, Paleoceanography 9 (1994) 677–692.

[53] R.M. Hotinski, K.L. Bice, L.R. Kump, R.G. Najjar, M.A. Arthur, Ocean stagnation and end-Permian anoxia, Geology 29 (2001) 7–10.

[54] G.J. Retallack, J.J. Veevers, R. Morante, Global coal gap between Permian–Triassic extinction and Middle Triassic recovery of peat-forming plants, Geol. Soc. Amer. Bull. 108 (1996) 195–207.

[55] E.W. Bolton, R.A. Berner, S.T. Petsch, The weathering of sedimentary organic matter as a control on atmospheric O2: II. Theoretical modeling, Am. J. Sci. 306 (2006) 575–615.

[56] S.L. Kamo, G.K. Czamanske, Y. Amelin, V.A. Fedorenko, D.W. Davis, V.R. Trofimov, Rapid eruption of Siberian flood-volcanic rocks and evidence for coincidence with the Permian–Triassic boundary and mass extinction at 251 Ma, Earth Planet. Sci. Lett. 214 (2003) 75–91.

[57] A.R. Basu, R.J. Poreda, P.R. Renne, F. Teichmann, Y.R. Vasiliev, N.V. Sobolev, B.D. Turrin, High-He-3 plume origin and

temporal-spatial evolution of the Siberian flood basalts, Science 269 (1995) 822–825.
[58] P.R. Renne, A.R. Basu, Rapid eruption of the Siberian traps flood basalts at the Permo-Triassic boundary, Science 253 (1991) 176–179.
[59] P.B. Wignall, Large igneous provinces and mass extinctions, Earth-Sci. Rev. 53 (2001) 1–33.
[60] M.K. Reichow, A.D. Saunders, R.V. White, A.L. Al'Mukhamedov, A.Y. Medvedev, Geochemistry and petrogenesis of basalts from the West Siberian basin: an extension of the Permo-Triassic Siberian Traps, Russia, Lithos 79 (2005) 425–452.
[61] M.K. Reichow, A.D. Saunders, R.V. White, M.S. Pringle, A.I. Al'Mukhamedov, A.I. Medvedev, N.P. Kirda, $^{40}Ar/^{39}Ar$ dates from the West Siberian Basin: Siberian flood basalt province doubled, Science 296 (2002) 1846–1849.
[62] T.M. Gerlach, E.J. Graeber, Volatile budget of Kilauea volcano, Nature 313 (1985) 273–277.
[63] L.R. Kump, M.A. Arthur, Interpreting carbon-isotope excursions: carbonates and organic matter, Chem. Geol. 161 (1999) 181–198.
[64] P. VanCappellen, E.D. Ingall, Redox stabilization of the atmosphere and oceans by phosphorus-limited marine productivity, Science 271 (1996) 493–496.
[65] G.K. Czamanske, A.B. Gurevitch, V. Fedorenko, O. Simonov, Demise of the Siberian plume: paleogeographic and paleotectonic reconstruction from the prevolcanic and volcanic record, north-central Siberia, Int. Geol. Rev. 40 (1998) 95–115.
[66] B. Buffett, D. Archer, Global inventory of methane clathrate: sensitivity to changes in the deep ocean, Earth Planet. Sci. Lett. 227 (2004) 185–199.
[67] E.S. Krull, G.J. Retallack, H.J. Campbell, G.L. Lyon, delta C-13 (org) chemostratigraphy of the Permian–Triassic boundary in the Maitai Group, New Zealand: evidence for high-latitudinal methane release, N.Z. J. Geol. Geophys. 43 (2000) 21–32.
[68] R.A. Berner, The carbon and sulfur cycles and atmospheric oxygen from middle Permian to middle Triassic, Geochim. Cosmochim. Acta 69 (2005) 3211–3217.
[69] J.C. Zachos, L.R. Kump, Carbon cycle feedbacks and the initiation of Antarctic glaciation in the earliest Oligocene, Glob. Planet. Change 47 (2005) 51–66.
[70] L.R. Kump, M.A. Arthur, M.E. Patzkowsky, M.T. Gibbs, D.S. Pinkus, P.M. Sheehan, A weathering hypothesis for glaciation at high atmospheric pCO_2 during the Late Ordovician, Palaeogeogr. Palaeoclimatol. Palaeoecol. 152 (1999) 173–187.
[71] A. Hallam, P.B. Wignall, Mass extinctions and sea-level changes, Earth-Sci. Rev. 48 (1999) 217–250.
[72] S. Pruss, D.J. Bottjer, Early Triassic trace fossils of the western United States and their implications for prolonged environmental stress from the end-Permian mass extinction, Palaios 19 (2004) 551–564.
[73] A.C. Maloof, D.P. Schrag, J.L. Crowley, S.A. Bowring, An expanded record of Early Cambrian carbon cycling from the Anti-Atlas Margin, Morocco, Can. J. Earth Sci. 42 (2005) 2195–2216.
[74] L.R. Kump, Interpreting carbon-isotope excursions — Strangelove oceans, Geology 19 (1991) 299–302.
[75] K.J. Hsü, J.A. McKenzie, A "Strangelove" ocean in the earliest Tertiary, in: E.T. Sundquist, W.S. Broecker (Eds.), The Carbon Cycle and Atmospheric CO_2: Natural Variations Archean to Present, American Geophysical Union, Washington, D.C., 1985, pp. 487–492.
[76] A.E. Kontorovich, A.V. Khomenko, L.M. Burshtein, I.I. Likhanov, A.L. Pavlov, V.S. Staroseltsev, A.A. Ten, Main oil-source formations of the West Siberian basin, Pet. Geosci. 3 (1997) 359–369.
[77] A.V. Ivanov, S.V. Rasskazov, G.D. Feoktistov, H. He, A. Boven, $^{40}Ar/^{39}Ar$ dating of Usol'skii sill in the south-eastern Siberian Traps large igneous province: evidence for long-lived magmatism, Terra Nova 17 (2005) 203–208.
[78] R. Mundil, K.R. Ludwig, I. Metcalfe, P.R. Renne, Age and timing of the Permian mass extinctions: U/Pb dating of closed-system zircons, Science 305 (2004) 1760–1763.
[79] S.A. Bowring, D.H. Erwin, Y.G. Jin, M.W. Martin, K. Davidek, W. Wang, U/Pb zircon geochronology and tempo of the end-Permian mass extinction, Science 280 (1998) 1039–1045.
[80] D.J. Lehrmann, J.Y. Wei, P. Enos, Controls on facies architecture of a large Triassic carbonate platform: the Great Bank of Guizhou, Nanpanjiang Basin, South China, J. Sediment. Res. 68 (1998) 311–326.